R-matrix treatment of high-energy electron-impact excitation processes: The generalized oscillator strengths for the Na 3*s*-3*p* and 2*p*-3*s* transitions

Xiaoying Han,[1,*] Yueming Li,[1] Hong Zhang,[1] and Jun Yan[1,2]
[1]*The Key Laboratory of Computational Physics, Institute of Applied Physics and Computational Mathematics, Beijing 100088, China*
[2]*Center for Applied Physics and Technology, Peking University, Beijing 100871, China*

JiaMing Li
Department of Physics, Shanghai Key Laboratory for Laser Fabrication and Material Science, Shanghai Jiaotong University, Shanghai 200030, China
The Key Laboratory of Atomic and Molecular Nanosciences of the Ministry of Education, Department of Physics, Tsinghua University, Beijing 100084, China

Lan Voky
LERMA, UMR 8112 du CNRS, Observatoire de Paris, 92915 Meudon Cedex, France
(Received 23 June 2008; published 3 November 2008)

High-energy electron-impact excitation cross sections are directly proportional to the generalized oscillator strengths (GOS's) of the target (an atom or molecule). In the present work, the GOS's for the Na 3*s*-3*p* and 2*p*-3*s* transitions are calculated by using the updated *R*-matrix codes. The present results for the 3*s*-3*p* transition are in good agreement with the experimental measurements at 1 keV incident energy. For the 2*p*-3*s* resonance transition, the present results are larger than the measurements at 1 keV incident energy. The difference is discussed. The important role of the inner shell electron correlations is elucidated. The positions of the first and second GOS minimums and maximums for these two transitions are reported. The dependence of the GOS minimum and maximum positions on the increasing incident energies are discussed.

DOI: 10.1103/PhysRevA.78.052702 PACS number(s): 34.80.Dp, 31.15.ag

I. INTRODUCTION

Electron-impact excitation (EIE) processes are of fundamental and practical importance. The total and differential cross sections of the EIE process are indispensable physical parameters in plasma physics, atmospheric physics, and astrophysics. For high enough but nonrelativistic incident energies, the first Born approximation (FBA) is applicable [1–3]. Within the FBA, the differential cross section (DCS) is proportional to the generalized oscillator strength (GOS), which is a function of the momentum transfer K and energy transfer ΔE. More specifically, the GOS is proportional to the square of the corresponding transition matrix element. For a certain transition, the transition matrix element may change sign when smoothly varying with the increasing momentum transfers. At the positions where the matrix elements change sign, there exist the GOS minimums.

The EIE process of the sodium atom has been the object of numerous experimental and theoretical investigations both for its existence in the atmosphere and for its hydrogenlike electronic structure. Experimentally, the DCS's and GOS's for the Na $[2p^6 3s]\ ^2S^e \rightarrow [2p^6 3p]\ ^2P^o$ excitation, which is called the 3*s*-3*p* transition, have been reported at incident energies from 10 eV to 1 keV over a large scattering angle range [4–9]. In addition, Ref. [9] reported the GOS's for the Na $[2p^6 3s]\ ^2S^e \rightarrow [2p^5 3s^2]\ ^2P^o$ resonance excitation measured at 1 keV incident energy, which is called the 2*p*-3*s* transition. Theoretically, although the electronic structure of the sodium ground state is a neonlike atomic core plus a 3*s* valence electron, because of the strong electron correlations between the core and the valence electrons, a sophisticated theoretical treatment is required, especially for the inner shell electron excitations. The theoretical investigations for the 3*s*-3*p* transition have been reported by the formalism of close coupling [10], distorted wave [11], Glauber approximation [12], self-consistent-field (SCF) Hartree-Fock approximation [9,13,14], and random phase approximation with exchange (RPAE) [13]. For the 2*p*-3*s* resonance transition, to our knowledge, only the GOS's calculated by using SCF Hartree-Fork wave functions within the frozen-core approximation [9] were reported, which were generally smaller than the experimental measurements [9] by about 30%.

In this work, we calculate the GOS's for the Na 3*s*-3*p* and 2*p*-3*s* transitions over large momentum transfer ranges by using the updated *R*-matrix codes. Based on a set of good orbital and configuration bases, the electron correlations, e.g., the monopole and higher multipole polarization effects, between the core and the excited electron can be considered adequately. For the 3*s*-3*p* transition, the present calculated GOS's agree well with the experimental measurements at 1 keV [9]. Our first GOS minimum and maximum positions accord well with the RPAE results [13] and the second GOS minimum and maximum positions are predicted. The dependence of the extracted experimental GOS minimum and maximum positions on the increasing incident energies is discussed.

For the 2*p*-3*s* resonance excitation, its GOS density can be fitted to Fano profiles [15,16]. The present calculated GOS's are generally larger than the experimental measure-

*hanxiaoying@tsinghua.org.cn

ments at 1 keV incident energy [9] except an accordance at $K^2=1.8$ a.u. Through detailed discussions about such as the applicability condition of the FBA, the important role of the inner shell electron correlations, and the high qualities of the relevant wave functions used in our calculations, the reliability of the present calculations is demonstrated and the difference is analyzed. The first and second GOS minimum and maximum positions are predicted. The different manners by which the Fano profile index q_i changes sign with the increasing K^2 are displayed.

II. THEORETICAL TREATMENT

The GOS $F(\Delta E,K)$ of the target is defined as [3] (atomic unit is used throughout the paper if not specified)

$$F(\Delta E,K)=\frac{2\Delta E}{K^2}\left|\left\langle \varphi_{T'}(\tilde{L}'\tilde{S}'\tilde{\pi}')\left|\sum_{\alpha=1}^{N} e^{i\vec{K}\cdot\vec{r}_\alpha}\right|\varphi_T(\tilde{L}\tilde{S}\tilde{\pi})\right\rangle\right|^2. \tag{1}$$

Here ΔE is the energy transfer, $\vec{K}$ is the momentum transfer of the impact electron, $\vec{r}_\alpha$ is the coordinate of the α electron in the target relative to the centroid of the target, and $\phi_T(\tilde{L}\tilde{S}\tilde{\pi})$ and $\phi_{T'}(\tilde{L}'\tilde{S}'\tilde{\pi}')$ are the initial and final state wave functions of the target with the definite angular momentum $\tilde{L}(\tilde{L}')$, spin $\tilde{S}(\tilde{S}')$, and parity $\tilde{\pi}(\tilde{\pi}')$. The DCS of the target at high incident energy is proportional to the GOS.

$$\frac{d\sigma}{d\Omega}=\frac{2}{\Delta E}\frac{k'}{k}\frac{F(\Delta E,K)}{K^2}. \tag{2}$$

In the limit of zero momentum transfer, the GOS becomes equal to the optical oscillator strength (OOS) [3]. This relation connects the high-energy electron-impact excitation process with the photoabsorption process.

In order to accurately calculate the GOS of the target, we have developed the *R*-matrix codes [17–19] to evaluate the transition matrix of the target in formula (1). Since the detailed descriptions of the *R*-matrix method have been presented in the previous works [20–26], only a brief outline will be given here. In the *R*-matrix method, the wave functions in a channel, including the Rydberg, adjacent continuum and autoionization state wave functions, are expanded on equal footing. This method begins by partitioning the subconfiguration space of the excited electron into two regions by a sphere of radius a centered on the nucleus. The value of a is chosen such that the exchange interactions between the excited electron and the core electrons are negligible for $r\geqslant a$, where r is the distance of the excited electron relative to the centroid of the core. Thus in the external region ($r\geqslant a$), the excited electron mainly "feels" the Coulomb potential as well as the long-range static polarization potential, and the wave functions of the excited electron satisfy a set of coupled two-order differential equations.

In the inner region ($r\leqslant a$), the interactions between the excited electron and the core electrons involve the electron exchange and correlation interactions. This is a many-body problem and is solved variationally as a whole to obtain the logarithmic derivative boundary matrix $\Re(E)$ on the *R*-matrix box surface (i.e., $r=a$). By the variational method, the electron correlations of the *N*-electron system, including the core and the excited electron, are calculated adequately [27,28]. The wave functions Ψ of eigenenergy E for the *N*-electron system are expanded as

$$\Psi=\sum_k A_{Ek}\Psi_k. \tag{3}$$

Here Ψ_k is a set of energy-independent configuration bases, which is expanded as

$$\Psi_k=\mathcal{A}\sum_{ij} a_{ijk}\tilde{\Phi}_i(\vec{r}_1,\ldots,\vec{r}_\alpha,\ldots,\vec{r}_{N-1};\hat{r}_N,\sigma_N)\frac{1}{r_N}u_{ij}(r_N)+\sum_j b_{jk}\phi_j(\vec{r}_1,\ldots,\vec{r}_\alpha,\ldots,\vec{r}_N), \tag{4}$$

where $\mathcal{A}$ is the antisymmetrization operator, which accounts for the electron exchanges between the core electrons and the excited electron; $\vec{r}_\alpha$ is the coordinate of the α electron in the core; u_{ij} is the continuum orbital basis; φ_j is completely formed by the bound orbitals to ensure the completeness of the wave functions of the *N*-electron system and take account of the electron correlations within the reaction zone; and $\tilde{\Phi}_i$, which has definite total angular momentum, spin, and parity, is the *i*th channel wave function obtained by coupling the core wave functions with the angular and spin wave functions of the *N*th electron. More specifically, the core wave functions are usually written as the linear superpositions of a set of basis configurations to take into account the electron correlations by a self-consistent multiconfiguration interaction method. These basis configurations are constructed as antisymmetrized product-type wave functions by a set of bound orbital bases with appropriate angular momentum couplings. The radial wavefunctions of these bound orbital bases are the linear superpositions of the Slater-type orbital bases [29].

In this work, we adopt the following orbital bases: $1s,2s,2p,3s,3p,3d,4s,4p,4d,\bar{5}s,\bar{5}p,\bar{5}d$ [30]. Here $(\bar{5}s,\bar{5}p,\bar{5}d)$ are the polarized pseudo-orbitals [31–35], by which the static polarization effects can be considered sufficiently. For such orbital bases, the present *R*-matrix box radius a is chosen to be 29.2 a.u. Based on this set of orbital bases we carefully choose 61 core states arising from the four kinds of configurations: $2p^6,2p^5nl,2p^4nln'l'$, $2p^3nln'l'n''l''$, which include the ground, and the singly, doubly, and triply excited core states. Table I shows the present calculated lowest nine energy levels of the core (Na^+) based on the above orbital and configuration bases. All the energy levels agree well with the NIST values [36] within 1%. Through these core states, the monopole and higher multipole polarization effects with the exchange correlations between the core electrons and the excited electron can be considered. Thus, the calculated lowest ionization energy of ground $Na[2p^63s]\ ^2S^e$ converges to 0.3793 Ry, which is in good agreement with the NIST value 0.3777 Ry [36] by about 0.4%. The calculated energy level of $Na[2p^63p]\ ^2P^o$ state converges to 0.2221 Ry, which agrees well with the NIST value 0.2231 Ry by about 0.4%. The good conver-

TABLE I. Our calculated lowest nine energy levels of the core (Na^+) relative to the energy level of the Na^+ ground state $[2p^6]\ ^1S^e$ (in Rydbergs).

No.	Core state	NIST data [36]	This work	Δ^a
1	$2p^6\ ^1S^e$			
2	$2p^5 3s\ ^3P^o$	2.4142	2.4029	−0.468%
3	$2p^5 3s\ ^1P^o$	2.4491	2.4322	−0.690%
4	$2p^5 3p\ ^3S^e$	2.6720	2.6755	0.131%
5	$2p^5 3p\ ^3D^e$	2.7087	2.7135	0.177%
6	$2p^5 3p\ ^1D^e$	2.7264	2.7272	0.029%
7	$2p^5 3p\ ^1P^e$	2.7328	2.7341	0.048%
8	$2p^5 3p\ ^3P^e$	2.7347	2.7340	−0.026%
9	$2p^5 3p\ ^1S^e$	2.8145	2.8203	0.206%

[a]Percentage difference between our calculation results and the NIST data [36], $(E_{theor}-E_{NIST})/E_{NIST}$.

gence of the energy levels manifests that not only the respective good convergence of Na^+ and Na systems, but also the good balance between the bound and continuum states are obtained.

After obtaining the initial and final state wave functions, the GOS can be calculated by using the updated *R*-matrix codes [17–19], which were based on the traditional *R*-matrix codes [20–26], while all the related subroutines for calculating the radiative dipole transition matrices were modified by substituting the operator $\Sigma_\alpha e^{i\vec{K}\cdot\vec{r}_\alpha}$ for the dipole operator $\Sigma_\alpha \vec{r}_\alpha$, and all the corresponding transition matrix elements of the radial and angle integrals were rearranged. In our previous works [17–19], we have reported the GOS's for the two-electron helium system. In the present work, the codes are furthermore extended to calculate the GOS for any electron system.

III. RESULTS AND DISCUSSION

A. 3*s*-3*p* transition

Using the updated *R*-matrix codes and based on the above orbital and configuration bases, we calculate the GOS's for the Na 3*s*-3*p* transition by evaluating the transition matrices. In the limit of $K^2 \to 0$, the present calculated GOS converges to 0.966, which accords well with the experimental OOS 0.975 [37–39] within 1%. In Fig. 1, the present calculated GOS's are compared with other theoretical and experimental results over 0.001 a.u. $\leqslant K^2 \leqslant 1$ a.u. The present results agree well with the experimental results at 1 keV ($R=500$, $R=E_i/\Delta E$ is the ratio of the incident energy to the excitation energy) [9]. The agreement demonstrates the high accuracies of $Na[2p^6 3s]\ ^2S^e$ and $Na[2p^6 3p]\ ^2P^o$ state wave functions and manifests that at 1 keV ($R=500$) and in this K^2 range the FBA is applicable. The present results agree well with the theoretical results of the RPAE method [13] but are larger than the results of the SCF method [14]. The discrepancy manifests that the electron correlations play an important role even for the valence electron excitation. The measurements of Marinkovic *et al.* at 10, 20, and 54.4 eV [8] are

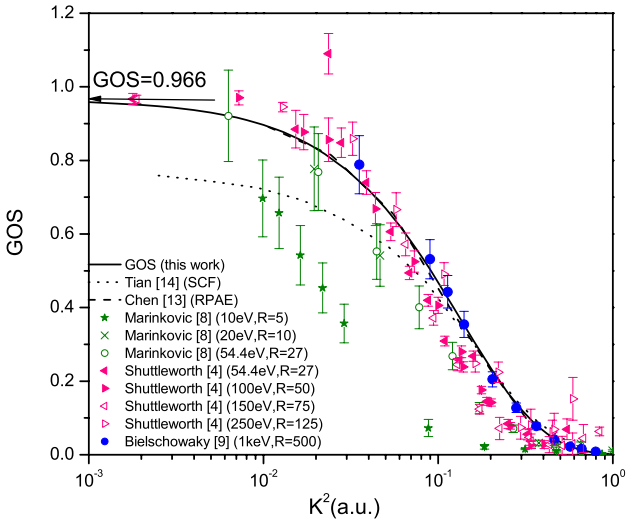

FIG. 1. (Color online) The GOS's for the 3*s*-3*p* transition over 0.001 a.u. $\leqslant K^2 \leqslant 1$ a.u. (—), our calculated GOS's by the updated *R*-matrix codes; (···), the SCF results [14]; (– –), the RPAE results [13]; (★, ×, ○), the measurements of Marinkovic *et al.* [8] at 10, 20, and 54.4 eV; (◀,▶,◁,▷), the measurements of Shuttleworth *et al.* [4] at 54.4, 100, 150, and 250 eV; (●), the measurements of Bielschowsky *et al.* [9] at 1 keV. $R=E_i/\Delta E$ is the ratio of the incident energy to the excitation energy.

lower than the FBA results and the measurements at 1 keV. The difference reduces as the incident energy increases. The measurements of Shuttleworth *et al.* at 54.4, 100, 150, and 250 eV [4], are close to each other and the results at lower incident energies are slightly smaller than those at higher incident energies. The variation of the measurements with the increasing incident energies illustrates the convergence procedure to the FBA. More specifically, Fig. 1 shows that for $R>50$ the measurements have generally converged to the present FBA results: for $R=27$, the results of Marinkovic *et al.* are smaller than the FBA results by about 20%, while the results of Shuttleworth *et al.* converge to the FBA results; the discrepancy between the two experiments at small K^2 has been discussed by Ref. [40] in detail.

In Fig. 2, the GOS's over 0.01 a.u. $\leqslant K^2 \leqslant 40$ a.u. are displayed. In this K^2 range, the GOS's generally decrease with the increasing K^2. Meanwhile, the GOS's present two minimums at about $K^2=1.578$ a.u. and $K^2=10.608$ a.u., respectively. These minimums result from the corresponding transition matrix elements changing sign during smoothly varying with the increasing K^2, which can be seen more evidently in the following discussions of the 2*p*-3*s* resonance transition. The present calculated first GOS minimum and maximum positions are in good accordance with those of the RPAE method [13]. The first minimum and maximum positions calculated within Hartree-Fock and frozen-core approximations [13] deviate our results and the PRAE results by about 10%–20%. The discrepancy further manifests the importance of the electron correlations, especially the inner shell electron correlations, for the valence electron excitation.

In Fig. 2, the variation of the experimental GOS minimum and maximum positions with the increasing incident energies

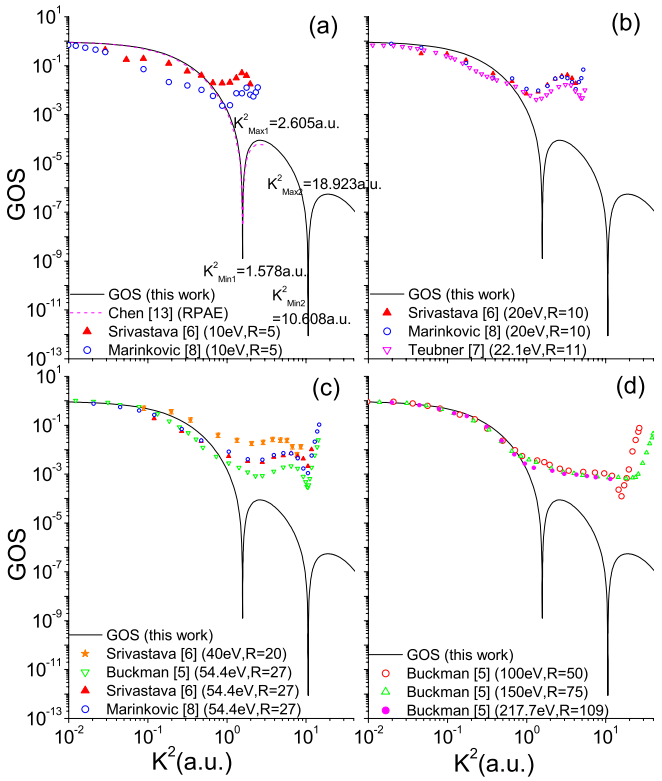

FIG. 2. (Color online) The variation of the experimental GOS minimum and maximum positions with the increasing incident energies. The available experimental values are roughly partitioned into four groups according to the incident energies as shown in the above four panels: (a) at E_i=10 eV; (b) At E_i=20, and 22.1 eV; (c) at E_i=40 and 54.4 eV; and (d) at E_i>100 eV.

is displayed. For clearer comparison, we partition the available measurements, only including those over K^2 range larger than 1 a.u., into four groups according to the incident energies: 10 eV, 20 eV, 54.4 eV, and >100 eV. The rough K^2 and scattering angles Ω corresponding to the first and second GOS minimums and maximums (labeled as Min1, Max1, Min2, Max2) of the measurements are extracted and listed in Table II. From Table II, it shows that Ω_{Min1}, Ω_{Max1}, and Ω_{Min2} generally decrease with the increasing E_i and converge to the FBA results. It is interesting that K^2_{Min1} is firstly smaller (e.g., for incident energies lower than 40 eV) and then becomes larger than the FBA K^2_{Min1} with the increasing E_i. Similar behaviors also exist for K^2_{Max1} and K^2_{Min2}. These interesting variations can be understood by the following relations between K^2, Ω, and E_i:

$$K^2 = 2[2E_i - \Delta E - 2\sqrt{(E_i - \Delta E)E_i}\cos\Omega]. \tag{5}$$

Formula (5) shows that K^2 increases with the increasing E_i and Ω ($0 \leqslant \Omega \leqslant 180$). Therefore, the nonmonotonic variation behaviors of K^2 are due to the competition between the increasing E_i and the decreasing Ω. It is expected that with the increasing incident energy higher than 100 eV, K^2_{Min1}, K^2_{Max1}, and K^2_{Min2} should decrease and converge to the FBA results. On the other hand, Fig. 2 shows that at large K^2, the experimental results are much larger than the FBA results. This large deviation is due to the failure of the FBA at the large K^2 range. While at higher incident energies, the K^2 range, where the FBA is applicable, becomes larger, which is illustrated by the longer and longer range overlaps between the experimental and FBA results from panel (a) to (d).

TABLE II. The K^2 (scattering angle Ω) corresponding to the first and second GOS minimum and maximum positions for the 3*s*-3*p* transition (in a.u. and deg units, respectively).

Experiment				
Incident energy	Min1	Max1	Min2	Max2
10 eV of Srivastava *et al.* [6]	0.9(70)	1.5(100)		
10 eV of Marinkovic *et al.* [8]	0.9(70)	1.8(110)	2.2(140)	
20 eV of Srivastava *et al.* [6]	1.0(50)	3.3(100)		
20 eV of Marinkovic *et al.* [8]	1.4(60)	2.8(90)	4.2(120)	
22.1 eV of Teubner *et al.* [7]	1.3(55)	3.1(90)	4.9(125)	
40 eV of Srivastava *et al.* [6]	2.0(50)	4.7(80)	7.7(110)	
54.4 eV of Srivastava *et al.* [6]	2.8(50)	6.5(80)	10.5(110)	
54.4 eV of Marinkovic *et al.* [8]	2.8(50)	5.2(70)	10.5(110)	
54.4 eV of Buckman *et al.* [5]	2.3(45)	6.5(80)	10.5(110)	
100 eV of Buckman *et al.* [5]			15.8(95)	
Theory				
HFA of Chen *et al.* [13]	1.963	2.856		
RPAE of Chen *et al.* [13]	1.583	2.592		
This work (FBA)	1.578	2.605	10.608	18.923
	(8.4)[a]	(10.8)	(21.9)	(29.4)

[a]The scattering angles correspond to 1 keV incident energy.

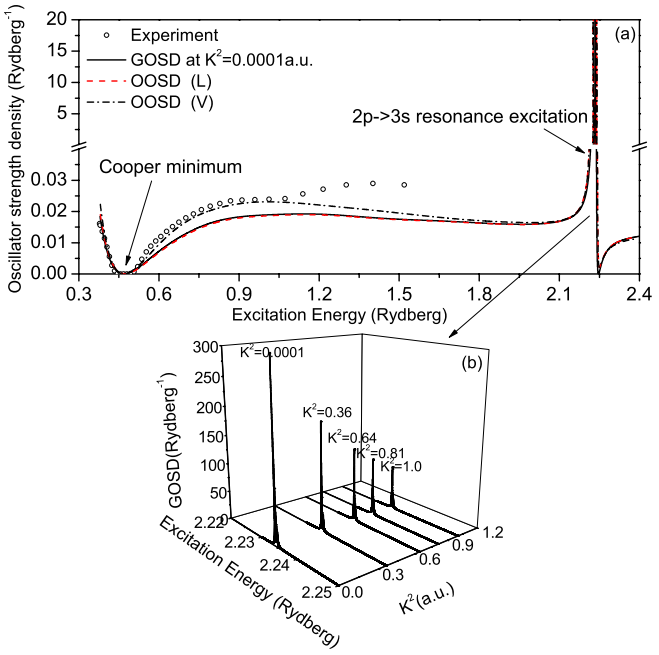

FIG. 3. (Color online) (a) The GOSD's and OOSD's for the $2p$-$3s$ resonance transition above the first ionization threshold of the ground Na; (b) the GOSD surface of the $2p$-$3s$ resonance transition. (—) our calculated GOSD's by the updated R matrix; (– –) our calculated OOSD's in the length form by the Breit-Pauli R-matrix [30]; (–·–) our calculated OOSD in the velocity form by the Breit-Pauli R-matrix [30]; (○) experimental measurements [41]; our previous work has provided an answer for the abnormal bump of the measurements in the energy range larger than 1 Ry [30].

B. $2p$-$3s$ transition

Based on the same orbital and configuration bases, the GOS's for the $2p$-$3s$ resonance excitation are calculated over a large momentum transfer range. Because the final state $\mathrm{Na}[2p^5 3s^2]\,{}^2P^o$ is the first autoionization state above the first ionization threshold of ground Na, its GOS density (GOSD) curves (as shown in Fig. 3) can be fitted to Fano profiles as [15,16]

$$\frac{dF(\Delta E,K)}{dE} = \sum_i F_{ai}[|q_i \sin\Delta_i - \cos\Delta_i|^2 - 1] + F_c(E)$$
$$= \sum_i F_{ai}\left[\frac{(q_i+\varepsilon_i)^2}{1+\varepsilon_i^2} - 1\right] + F_c(E). \quad (6)$$

Here $F_c(E)$ is the GOSD of the total continuum background, which includes both parts that do and do not interfere with resonances; F_{ai} represents the relevant continuum interfering with the ith resonance; Δ_i is the phase parameter due to configuration interaction; $\varepsilon_i = -\cot\Delta_i = (E-E_{ri})/(\Gamma_i/2)$ stands for the departure of the excitation energy E from the resonance energy E_{ri} scaled by the half linewidth $\Gamma_i/2 = \pi|V_E|^2$; here $V_E = (\psi_E|H|\phi)$ is the Hamiltonian matrix element between the continuum state ψ_E and the discrete state ϕ; $q_i = (\Phi|T|\phi_i)/[\pi V_E^*(\psi_E|T|\phi_i)] = (\Phi|T|\phi_i)/[(\psi_E|T|\phi_i)\sqrt{\Gamma_i/2}]$ is a line profile index which represents the ratio of the transition amplitude of the "modified" discrete state Φ to that of the relevant continuum state; ϕ_i is the initial state of the transition. For a specific resonance, the integrated GOS F_i of the modified discrete state Φ is expressed as

$$F_i = \frac{\pi\Gamma_i}{2} F_{ai}|_{E=E_{ri}} q_i^2, \quad (7)$$

since F_{ai} is nearly a constant with E. The integrated resonance strength S_i of the modified discrete state and the relevant continuum is

$$S_i = \frac{\pi\Gamma_i}{2} F_{ai}|_{E=E_{ri}} (q_i^2 + 1). \quad (8)$$

The integrated strength F_{ic} of the relevant continuum is

$$F_{ic} = S_i - F_i = \frac{\pi\Gamma_i}{2} F_{ai}|_{E=E_{ri}}. \quad (9)$$

The present fitted resonance energy position of the $\mathrm{Na}[2p^5 3s^2]\,{}^2P^o$ state is at 2.23 Ry, which agrees with the NIST value 2.27 Ry [36] by about 1.8%.

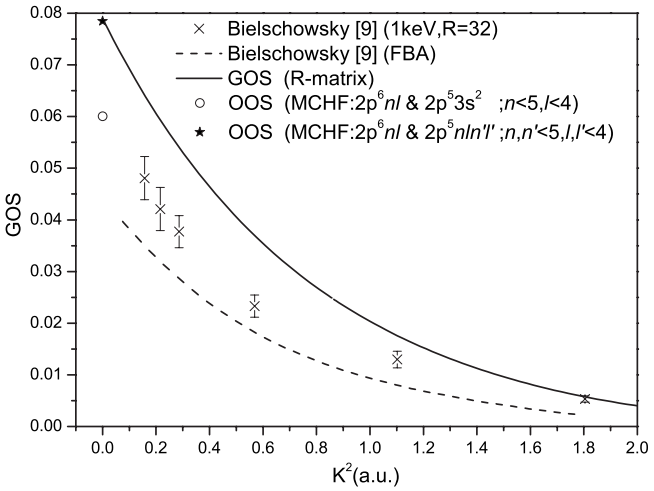

FIG. 4. The GOS's for the $2p$-$3s$ transition. (—) Our calculated GOS's (i.e., F_i) by the updated R-matrix codes; (○) our calculated OOS by the MCHF method based on basis I ($2p^6nl$ and $2p^5 3s^2$; $n<5$, $l<4$); (★) our calculated OOS by the MCHF method based on basis II ($2p^6nl$ and $2p^5 nln'l'$; $n,n'<5$, $l,l'<4$); (×) the measured GOS's of Bielschowsky at 1 keV [9]; (– –) the theoretical results of Bielschowsky [9] by using self-consistent-field Hartree-Fork wave functions within the frozen-core and FBA approximation.

In Fig. 4, the present calculated GOS's F_i for the $2p$-$3s$ resonance transition are compared with the experimental results measured at 1 keV ($R=32$) over 0 a.u. $\leqslant K^2 \leqslant 2$ a.u. [9]. As shown in Fig. 4, the experimental results are generally smaller than the present R-matrix results by about 30%–50% except an accordance at $K^2=1.8$ a.u. This large difference is interesting because we note that for the $3s$-$3p$ transition, at $E_i \geqslant 54.4$ eV ($R \geqslant 27$) the measurements are at most smaller than the FBA results by 20%. On the other hand, from an experimental aspect, it is known that at certain incident energy, if the FBA is applicable at large momentum transfer, its applicability at small momentum transfer is guaranteed. From the theoretical aspect, the present GOS calculations are

based on the same set of initial and final state wave functions and what changed is only the $\vec{K}$ in formula (1), and the good agreement of the GOS variation with K^2 of the $3s$-$3p$ transition between our theoretical results and the experimental measurements [9] has proven the credibility of our updated R-matrix codes to some extent. Therefore, we think that the accordance at about $K^2=1.8$ a.u. may be an occasional occurrence. However, what is the reason for the large difference between the present theoretical results and the measurements at small K^2?

Note that, our present calculations are based on a set of good core orbital bases, a large configuration space for the core states, and hundreds of channel wave functions for the whole system. This ensures the good consideration of the electron correlations. For example, for the $2p^53s^2$ resonance state, the channel wave functions involving the triply excited core states ($2p^3nln'l'n''l''$) are included to ensure the monopole and high-order multipole polarization effects are taken into account. The set of wave functions based on the same bases have been used in our previous work [30,42] successfully to reproduce the Cooper minimum, which agrees well with the experimental measurements [41]. This agreement manifested the high quality of the relevant bound state ($2p^63s$) and continuum state ($2p^6\varepsilon p$) wave functions involved in the present work. In Fig. 3(a), the present calculated GOSDs at $K^2=0.0001$ a.u. are compared with the OOSD's (i.e., the photoionization cross sections) over the excitation energy range including the Cooper minimum and the ($2p^23s^2$) resonance. It shows that in this energy range the OOSD's in the length and the velocity forms agree well with each other except an energy range 0.6 Ry$\sim$1.8 Ry beyond the resonance. More specifically, around the $2p^53s^2$ resonance, the OOSD's in the length and velocity forms merge together well, which verifies the high quality of the resonance state wave function. The present calculated GOSD at $K^2=0.0001$ a.u. using the same set of wave functions as those of the OOSD's agree well with the OOSD's as shown in Fig. 3(a). With the increasing K^2, the GOSD surfaces are obtained by using the same set of wave functions as shown in Fig. 3(b), which should be of the same accuracy as that of the OOSD's. Being fitted to Fano profiles, the GOS's F_i of this resonance at different K^2 are obtained as shown in Fig. 4. In the limit of $K^2\rightarrow 0$, our calculated GOS is equal to our calculated OOS value 0.079.

In addition, we calculate the OOS for the $2p$-$3s$ resonance transition by the multiconfiguration Hartree-Fork (MCHF) method with relativistic corretions [43–45]. More specifically, we choose two sets of configuration bases: the core of basis I ($2p^6nl$ and $2p^53s^2$; $n<5$, $l<4$) is frozen and the core of basis II ($2p^6nl$ and $2p^5nln'l'$; $n,n'<5$, $l,l'<4$) is relaxed. Because of the narrow linewidth of the resonance, the present MCHF calculations do not consider the continuum background interactions. The calculated OOS (0.078) based on basis II accords well with our R-matrix result (0.079). The calculated OOS (0.06) based on basis I is smaller than the result of basis II by about 30%. The difference between the results based on basis I and basis II elucidates the important role of the inner shell electron correlations for the inner shell electron excitations. Note that, the OOS of basis I seems to agree with the measurements at $K^2\rightarrow 0$, but according to the above discussions we think this is only an accidental appearance. The MCHF calculations provide independent evidence for the reliability of our GOS calculations. The theoretical results of Bielschowsky *et al.* [9] using SCF Hartree-Fork wave functions within the frozen-core approximation are generally smaller than the experimental results by about 30% and smaller than our MCHF results based on basis I and basis II by about 40% and 50%, respectively. The difference between the results of basis I and the theoretical results of Bielschowsky *et al.* may result from the configuration interaction considered in our calculations.

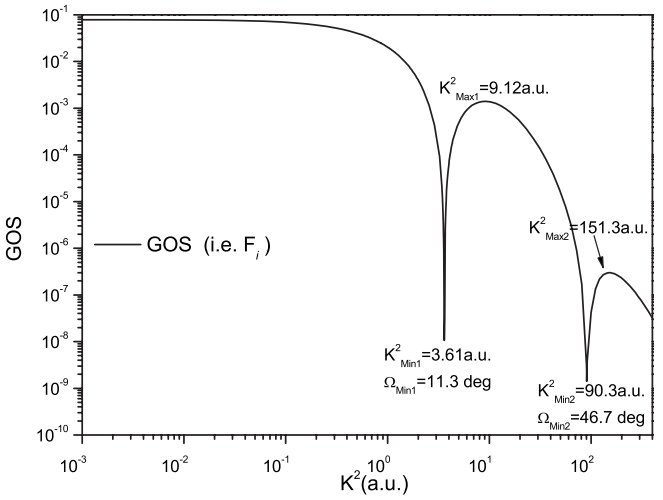

FIG. 5. The present calculated GOS's F_i for the $2p$-$3s$ transition over the 0.001 a.u.$\leqslant K^2\leqslant$400 a.u. range. The scattering angles Ω correspond to $E_i=2$ keV ($R=65$).

The above detailed discussions elucidate the important role of the inner shell electron correlations and demonstrate the reliability of the present calculation results. Let us return to analyze the difference between our calculated GOS's and the measurements. Noted that the excitation energy of the $2p-3s$ transition is about 15 times higher than that of the $3s$-$3p$ transition and for the same incident energy $E_i=1$ keV their R's are, respectively, equal to 32 and 500, therefore, one possible explanation for the difference may be the failure of the FBA. To clearly elucidate the convergent procedure to the FBA for the inner shell excitations of Na, we suggest a further high-energy (higher than 1 keV) experimental study with high resolution.

Figure 5 shows the present calculated GOS's for the $2p$-$3s$ resonance excitation over the 0.001 a.u.$\leqslant K^2\leqslant$400 a.u. range. In this K^2 range, the GOS's present two minimums at about $K^2=3.61$ a.u. and $K^2=90.3$ a.u.. Compared with the GOS minimum and maximum positions for the $3s$-$3p$ transition, those for the $2p$-$3s$ transition correspond to larger K^2 values. The different extremum positions are due to the different relative phase shifts between the same initial state and the different final states.

In Fano profiles, the value of the line profile index $q_i=(\Phi|T|\phi_i)/[(\psi_E|T|\phi_i)\sqrt{\Gamma_i/2}]$ is the ratio of the transition probabilities to the "modified" discrete state Φ and those to a bandwidth Γ_i of relevant continuum state ψ_E; here Γ_i is nearly a constant with the increasing K^2; for the $2p$-$3s$ reso-

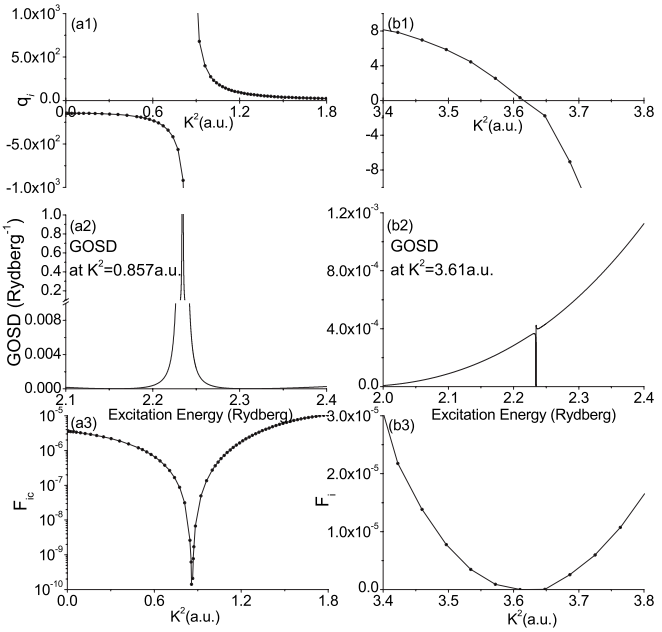

FIG. 6. [(a1) and (b1)] The Fano parameters q_i vary as a function of K^2. [(a3) and (b3)] The integrated strengths F_{ic} and F_i for the $2p$-$3s$ resonance transition vary as a function of K^2. [(a2) and (b2)] The GOSD curves correspond to the $q_i \to \infty$ and $q_i \to 0$, respectively.

nance transition, our fitted $\Gamma_i/2$ is equal to 8.28×10^{-5} Ry. The value of q_i may change sign when $(\Phi|T|\phi_i)$ and $(\psi_E|T|\phi_i)$ change sign during smoothly varying with the increasing K^2. Since the two transition matrix elements are, respectively, numerator and denominator, the value of q_i changes sign by different manners as shown in Fig. 6. In Fig. 6(a), the value of q_i changes from negative infinite to positive infinite when $(\psi_E|T|\phi_i)$ changes sign, i.e., when F_{ic} passes through zero for F_{ic} is proportional to the square of $(\psi_E|T|\phi_i)$. At the turning point where q_i is equal to infinity, the profile of the corresponding GOSD curve displays a symmetry feature as shown in Fig. 6(a2). In Fig. 6(b), the value of q_i changes sign smoothly from negative to positive when $(\Phi|T|\phi_i)$ changes sign, i.e., when F_i passes through zero for F_i is proportional to the square of $(\Phi|T|\phi_i)$. At the point where q_i is equal to zero, the profile of the corresponding GOSD curve displays a window feature as shown in Fig. 6(b2). Figure 6 shows that $(\Phi|T|\phi_i)$ and $(\psi_E|T|\phi_i)$ change sign at different K^2 values, which results from the different phase shifts of different final states.

IV. CONCLUSION

Using the updated *R*-matrix codes, we calculate the GOS's for the Na $3s$-$3p$ and $2p$-$3s$ excitations. Based on a set of good orbital and configuration bases the electron correlations, especially the inner shell electron correlations, between the core and the excited electron are taken into account sufficiently.

For the $3s$-$3p$ transition, at E_i=54.4 eV (R=27), the measurements are smaller than our FBA results by about 20%, and at higher incident energies the measurements become closer to the FBA results, and at 1 keV (R=500) the measurements agree well with the FBA results. The present first GOS minimum and maximum positions for the $3s$-$3p$ transition agree well with the theoretical results of the RPAE method while they differ from the results calculated by Hartree-Fock and frozen-core approximations. The differences manifest that the inner shell electron correlations are important even for the valence electron excitations. The second GOS minimum and maximum positions are reported. Table II shows that the scattering angles Ω corresponding to the GOS minimums and maximums decrease with the increasing E_i and the corresponding K^2 firstly increase, and then are expected to decrease with the increasing E_i.

For the $2p$-$3s$ resonance transition, the present fitted energy position of Na$[2p^5 3s^2]\,^2P^o$ resonance state agree with the NIST value by about 1.8%. The experimental results at 1 keV (R=32) are smaller than the present calculated GOS's by about 30%–50% except an accordance at about K^2 =1.8 a.u. This difference is interesting compared to the difference (20% at most) between the measurements at E_i =54.4 eV (R=27) and our FBA results for the $3s$-$3p$ transition. The credibility of the modified codes is proved by the good convergence of the present calculated GOS's of the $3s$-$3p$ transition, and the high qualities of the relevant bound state $[2p^6 3s]\,^2S^e$, continuum state $[2p^6 \varepsilon p]\,^2P^o$, and resonance state $[2p^5 3s^2]\,^2P^o$ wave functions are verified by the good agreement between the OOSD's in the length and velocity forms around the resonance. By the additional MCHF calculations, the important role of the inner shell electron correlations is elucidated. The MCHF calculations provide independent evidence of the reliability of the present *R*-matrix calculations. Therefore, one possible explanation for the difference may be the failure of the FBA. To clearly illustrate the convergent procedure of the FBA for the inner shell electron excitations, we suggest a further detailed higher-energy experiment study with high resolution.

The first and second GOS minimum and maximum positions for the $2p$-$3s$ resonance transition are predicted. The two different manners, by which Fano profile index q_i changes sign with increasing K^2, are displayed. Based on the reliable modified codes and the wave functions with high qualities, the GOS's of the nondipole transitions, e.g., monopole and quadrupole transitions, can be readily obtained by evaluating the corresponding transition matrices and will be reported elsewhere.

ACKNOWLEDGMENTS

This work is supported by the National Basic Research Program (Grant No. 2005CB724500), the National Science Foundation of China (Grants No. 10734140, No. 10674021, No. 10674020, No. 10878008, and No. 10804012), National High-Tech ICF committee of China, and the Science and Technology Funds of CAEP (Grant No. 20060215).

[1] H. Bethe, Ann. Phys. **397**, 325 (1930).
[2] H. Bethe, Z. Phys. **76**, 293 (1932).
[3] M. Inokuti, Rev. Mod. Phys. **43**, 297 (1971).
[4] T. Shuttleworth, W. R. Newell, and A. C. H. Smith, J. Phys. B **10**, 1641 (1977).
[5] S. J. Buckman and P. J. O. Teubner, J. Phys. B **12**, 1741 (1979).
[6] S. K. Srivastava and L. Vuskovic, J. Phys. B **13**, 2633 (1980).
[7] P. Teubner, J. Riley, M. J. Brunger, and S. J. Buckman, J. Phys. B **19**, 3313 (1986).
[8] B. Marinkovic, V. Pejcev, D. Filipovic, I. Cadez, and L. Vuskovic, J. Phys. B **25**, 5179 (1992).
[9] C. E. Bielschowsky, C. A. Lucas, G. G. B. de Souza, and J. C. Nogueira, Phys. Rev. A **43**, 5975 (1991).
[10] I. E. McCarthy, J. Mitroy, and A. T. Stelbovics, J. Phys. B **18**, 2509 (1985).
[11] J. V. Kennedy, V. P. Myerscough, and M. R. C. McDowell, J. Phys. B **10**, 3759 (1977).
[12] H. R. J. Walters, J. Phys. B **6**, 1003 (1973).
[13] Z. Chen and A. Z. Msezane, Phys. Rev. A **61**, 030703(R) (2000).
[14] B. G. Tian and J. M. Li, Acta Phys. Sin. **33**, 1401 (1984).
[15] U. Fano, Phys. Rev. **124**, 1866 (1961).
[16] U. Fano and J. W. Cooper, Phys. Rev. **137**, A1364 (1965).
[17] Z. S. Yuan, X. Y. Han, X. J. Liu, L. F. Zhu, K. Z. Xu, L. Voky, and J. M. Li, Phys. Rev. A **70**, 062706 (2004).
[18] X. Y. Han, L. Voky, and J. M. Li, Chin. Phys. Lett. **21**, 54 (2004).
[19] X. Y. Han and J. M. Li, Phys. Rev. A **74**, 062711 (2006).
[20] P. G. Burke, A. Hibbert, and W. D. Robb, J. Phys. B **4**, 153 (1971).
[21] K. A. Berrington, P. G. Burke, J. J. Chang, A. T. Chivers, W. D. Robb, and K. T. Taylor, Comput. Phys. Commun. **8**, 149 (1974).
[22] K. A. Berrington, P. G. Burke, M. Dourneuf, W. D. Robb, K. T. Taylor, and L. Voky, Comput. Phys. Commun. **14**, 346 (1978).
[23] K. A. Berrington, P. G. Burke, K. Butler, M. J. Seaton, P. J. Storey, K. T. Taylor, and Y. Yan, J. Phys. B **20**, 6379 (1987).
[24] L. Voky, H. E. Saraph, W. Eissner, Z. W. Liu, and H. P. Kelly, Phys. Rev. A **46**, 3945 (1992).
[25] K. A. Berrington and A. E. Kingston, J. Phys. B **20**, 6631 (1987).
[26] K. A. Berrington, W. B. Eissner, and P. H. Norrington, Comput. Phys. Commun. **92**, 290 (1995).
[27] C. M. Lee (Jia-Ming Li), Phys. Rev. A **10**, 584 (1974).
[28] U. Fano and C. M. Lee (Jia-Ming Li), Phys. Rev. Lett. **31**, 1573 (1973).
[29] A. Hibbert, Comput. Phys. Commun. **9**, 141 (1975).
[30] X. Y. Han, X. Gao, J. M. Li, L. Voky, and N. Feautrier, Phys. Rev. A **74**, 062710 (2006).
[31] L. Voky, M. Dourneuf, and P. G. Burke, J. Phys. B **9**, 1065 (1976).
[32] J. F. Thornbury and A. Hibbert, J. Phys. B **20**, 6447 (1987).
[33] J. Yan, Y. Z. Qu, L. Voky, and J. M. Li, Phys. Rev. A **57**, 997 (1998).
[34] Y. H. Jiang, J. Yan, J. M. Li, J. F. Sun, and L. D. Wan, Phys. Rev. A **61**, 032721 (2000).
[35] Y. L. Peng, M. S. Wang, X. Y. Han, and J. M. Li, J. Phys. B **38**, 3825 (2005).
[36] NIST Atomic Spectra Database Levels Form (http://physics.nist.gov/PhysRefData/ASD/levels_form.html).
[37] C. E. Moore, *Atomic Energy Levels* (U.S. GPO, Washington, D.C., 1949).
[38] J. R. Link, J. Opt. Soc. Am. **56**, 1195 (1966).
[39] G. Stephenson, Proc. Phys. Soc., London, Sect. A **64**, 458 (1951).
[40] A. Z. Msezane, Z. F. Chen, and C. Handy, Phys. Rev. A **50**, 3905 (1994).
[41] R. D. Hudson*et al.*, J. Opt. Soc. Am. **57**, 651 (1967).
[42] X. Y. Han, X. L. Wang, L. Voky, N. Feautrier, and J. M. Li, Chin. Phys. Lett. **24**, 909 (2007).
[43] R. D. Cowan, *The Theory of Atomic Structure and Spectra* (University of California Press, Berkeley, CA, 1981).
[44] H. Zhang, Y. M. Li, J. Yan, and J. G. Wang, Phys. Rev. A **71**, 042705 (2005).
[45] H. Zhang, Y. M. Li, J. Yan, and J. G. Wang, Comm. Comp. Phys. **2**, 795 (2007).